Smoky Vehicle Detection Based on Range Filtering on Three Orthogonal Planes and Motion Orientation Histogram

HUANJIE TAO[ID], **(Member, IEEE), AND XIAOBO LU**[ID], **(Member, IEEE)**

School of Automation, Southeast University, Nanjing 210096, China
Key Laboratory of Measurement and Control of Complex Systems of Engineering, Ministry of Education, Southeast University, Nanjing 210096, China

Corresponding author: Xiaobo Lu (xblu2013@126.com)

ABSTRACT Smoky vehicle detection is an important task in reducing motor vehicle pollution. This paper presents a method to automatically detect smoky vehicles from the traffic surveillance videos. More specifically, the visual background extractor background subtraction algorithm and some rules are adopted to detect moving vehicle object and locate the key region at the back of the vehicle. Based on sufficient observations of the smoke characteristics in the real scene, three groups of features, including color moments (CMs) features, improved motion orientation histogram features, and the new model range filtering on three orthogonal planes (RF-TOP)-based features, are designed and proposed to distinguish smoky vehicles and non-smoke vehicles. The color information CM features are used as a preliminary sieve to filter out the samples that are obviously non-smoke regions. The other two groups of features are combined to one feature vector to obtain motion information and spatiotemporal information of the key region. Two strategies, including histogram and projection, are designed to extract discriminative dynamic features from the proposed model RF-TOP to characterize the key region. The pruning radial basis function neural network classifier is adopted to classify the extracted features. For the traffic surveillance videos in the daylight with sunny weather, the experimental results show that the proposed methods have better performances and work effectively with lower false alarm rates than existing methods, and the proposed method with histogram strategy achieves the best performance.

INDEX TERMS Smoky vehicle detection, color moments, motion orientation histogram, range filtering.

I. INTRODUCTION

Smoky vehicle is defined as the vehicle belching clearly visible exhaust fume and leaving a smoky trail at the back of the vehicle. The particulate matter (PM) in smoky vehicle diesel exhaust fume is harmful to the air and the human health, even causes upper respiratory problems and lung damage, especially for the exposed people [1], [2]. The smoky vehicle obviously fails to meet the emissions standard, and so it is necessary to detect the smoky vehicle and make further measurements and processing. The color of the smoky vehicle exhaust can be divided into white and black, which correspond to the white-smoke vehicle and the black-smoke

vehicle, respectively. This paper is focus on the black-smoke vehicle detection, since the black-smoke vehicle is more common and harmful.

To measure the smoky vehicle exhaust fume, the vehicle needs to be taken out of the traffic flow. Currently, the smoky vehicle detection methods in practical application can be divided into two strategies. 1) The traditional methods, such as, mass reporting, regular road inspection, night inspection, installing vehicle exhaust analysis device, sensor detection, etc. These methods can reduce the pollution of smoky vehicles to a certain extent. However, they also have some disadvantages. Firstly, for the method of mass reporting, the smoky

vehicles reported by the public are only a very small part of the total smoky vehicles. Secondly, for the method of installing the vehicle exhaust analysis device, the purchase and the follow-up maintenance of the devices are costly. It also needs more than one operators and authorities to be functional. Thirdly, due to the rapid growth of the vehicle ownership and the heavy traffic, these methods often need to invest many workers and financial resources. In summary all the above methods are with low efficiency and high cost. 2) Manual video surveillance. The workers watch the road surveillance videos in the monitoring room to detect smoky vehicles. However, if one worker often faces the duty of staring at hundreds of video surveillance screens, eyes will get tired quickly after few minutes, which may lead to wrong detections and miss detections. Actually it is a crucial challenge if a person has to monitor smoky vehicles effectively even between only two screens.

Starting from 2017, automatic smoky vehicle detection in surveillance video arises driven by the rapid developments of the computer vision technology and its wide applications in transportation and healthcare [3], [4]. The video cameras are increasingly prevalent on the road, and the image resolution continues to improve. These changes are important for automatic smoky vehicle detection. However, it still has many challenges: 1) High robustness. It should adapt to various complex environment, such as night time, bad weather (the foggy days and the rainy days). We also hope the surveillance videos can be directly used for smoky vehicles detection without relations to the installation position of the camera. 2) High real-time performance. To analyze multiple road surveillance videos simultaneously, it is important to satisfy the real-time performance. 3) Saving subsequent enforcement evidences. This means that the system can identify license plates and save relevant video clips automatically. In order to avoid illegal vehicle decks which caused invalid license plate information, this system can even add the face detection and recognition module.

To date, the smoky vehicle detection in surveillance videos based computer vision technology is still in its infancy and has many challenges. To the best of our knowledge, there are few published literatures so far on smoky vehicle detection. More specifically, Pyykonen *et al.* [5] first proposed a smoke detection and traffic pollution analysis system based on multiple cameras, including a far infrared camera and a high-resolution visible camera. However, the use and maintenance of multiple cameras will increase the cost, and it is poor in robustness, including the strategy of detecting exhaust pipe locations by searching hot spot in the thermal camera image, and the classification method by comparing the image graininess, intensity values and histogram features. It also needs calibrate far infrared images and high-resolution images together. Tao and Lu [6], [7] proposed two smoky vehicle detection methods, which used the multi-scale block Tamura features, local binary pattern (LBP), histograms of oriented gradients (HOG) and integral projection (IP). However, Tao's methods all did not consider the dynamic

features of the smoke, which easily lead to high false alarm rates.

Although there is little study so far on automatic smoky vehicle detection, there are lots of literatures on vision-based smoke and fire detection. More specifically, Yuan [8] proposed an accumulative motion model based on the integral image by fast estimating the motion orientation of the smoke. Gunay *et al.* [9] proposed an entropy-functional-based online adaptive decision fusion framework for video-based smoke and wildfire detection. However, Yuan and Gunay all assume that the smoke usually drifts upwards continually through hot airflow, but in smoky vehicle detection, the smoke emitted from vehicle exhaust hole does not drift upward. This makes the models ineffective in smoky vehicle detection. Chen *et al.* [10] proposed an early fire-alarm raising method by adopting a RGB (red, green, blue) model based chromatic and disorder measurement for extracting fire-pixels and smoke-pixels. However, in smoky vehicle detection, this method is ineffective since the colors of smoke and road are all dark gray. Toreyin *et al.* [11] used motion, flicker, edge blurring and color features for smoke detection. Variance of edge magnitudes was extracted for smoke detection. However, in smoky vehicle detection, it is difficult to extract pure motion and edge features of the smoke, since the smoke is connected with the vehicle objects all the time. Most extracted motion and edge features are vehicles' features. In addition, the smoke in smoky vehicle detection will not flickers like the smoke in fire detection. Tian *et al.* [12]–[14] proposed a series of image separation approaches which can be used for smoke detection. Tian's methods mainly focus on separating smoke component from the single frame image, and then extract texture features from the separated smoke component for smoke detection. However, these methods all did not consider the dynamic features of the smoke. In the smoky vehicle detection, it is important to extract dynamic features, since the road images and the black smoke images are similar, which easily leads to high false alarm rates. In summary, the application scenarios of the above methods are all smoke and fire detection, and still have some deficiencies when they are directly transplanted into the smoky vehicle detection.

To lower the false alarm rates, this paper presents an automatic smoky vehicle detection method based on Range Filtering on Three Orthogonal Planes (RF-TOP) and improved Motion Orientation Histogram (MOH). This method outperforms the state-of-the-art methods, and the main contributions are summarized below:

(1)We provide a labeled smoky vehicles and non-smoke vehicles dataset called SEU-SmokeVeh, which contains 157550 frames, including 151613 non-smoke frames and 5937 smoky frames.

(2)We propose a new model called RF-TOP to characterize the key region at the back of the detected vehicle objects, and two strategies including histogram and projection are designed to extract discriminative dynamic features to characterize the key region.
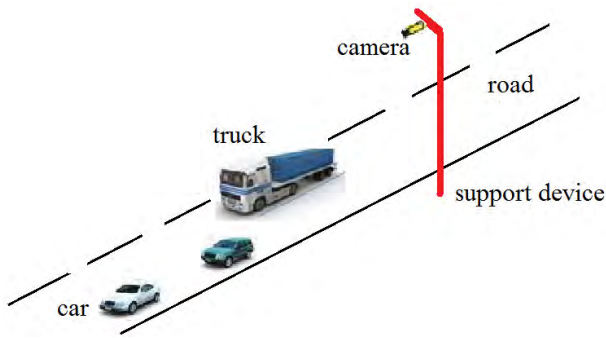
FIGURE 1. Detecting and tracking vehicles from the above angle in order to see different vehicle exhaust pipes and identify license plates, simultaneously.

FIGURE 2. A sketch map used to understand the concept of the key region. The key region is marked by the red box.

(3)We improve the original MOH features and propose the concept of main orientation to make the features have rotation invariance, which is useful in smoky vehicle detection.

(4)We design three groups of features to distinguish smoky vehicles and non-smoke vehicles, including CM, improved MOH and RF-TOP based features, which are used to obtain the color information, motion information and spatiotemporal information of the key region.

(5)We test the proposed method on the dataset SEU-SmokeVeh, and our method achieves the state-of-the-art experimental results, especially works effectively with lower false alarm rates than existing smoky vehicle detection methods and related smoke detection methods.

The remainder of this paper is organized as follows. In Section II, we will describe the method to obtain the key region. Section III will describe the designed three groups of features in detail. Section IV will introduce the Pruning Radial Basis Function Neural Network (P-RBFNN) classi-fier. In Section V, the experimental results and the compar-isons between our methods and the state-of-the-art methods will be presented. The conclusions are finally reported in Section VI.

II. KEY REGION LOCATION

The location of the camera is critical in the vehicle detection and tracking. In this paper, we detect and track the vehicle from the above angle, and see the back of the vehicle along the road to identify the license plate and detect possible smoke coming from the underneath of the vehicle. As shown in Fig.1, the installation makes it possible to monitor multiple lanes simultaneously.

Currently the accurate and robust vision-based moving objects detection is still a challenging task [16]. It mainly includes two kinds of the approaches. 1) A variety of back-ground subtraction algorithms [17], [18]. 2) Feature-based methods [19], [20]. In this paper the Visual Background Extractor (ViBe) background subtraction algorithm [18] is adopted, and it should be noted that other methods can also be used. In the practical applications of stationary camera, we use the strategy of nearest neighbor association to track the moving objects. Some other small tricks are also used.
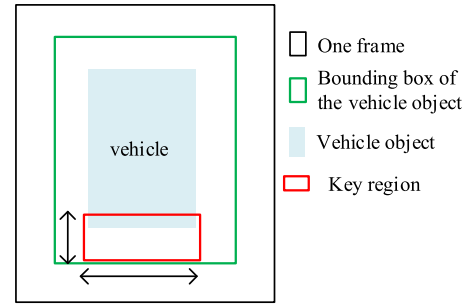
To remove the detected non-vehicle objects, the following two rules are designed:

$$
\begin{cases}
\text{Rule 1:} & S > S_{\min Veh} \\
\text{Rule 2:} & \dfrac{w_{movObj}}{h_{movObj}} \in [\delta_{\min Rat}, \delta_{\max Rat}]
\end{cases}
\tag{1}
$$

where S is the area of the detected moving object. $S_{\min Veh}$ denotes the minimum area of common vehicles, and it is recommended as 1500-2000 pixels. w_{movObj} and h_{movObj} are the width and height of the bounding box of the moving object, respectively. $[\delta_{\min Rat}, \delta_{\max Rat}]$ denotes the variation range of w_{movObj}/h_{movObj} for common vehicles, and it is recommended that $\delta_{\min Rat} \in [0.3, 0.5]$, $\delta_{\max Rat} \in [1.2, 1.4]$. In this paper, $S_{\min Veh} = 1800$, $\delta_{\min Rat} = 0.4$, $\delta_{\max Rat} = 1.3$, and the parameter setting is based on our empirical values and sufficient experiments. More than 98% of the vehicles should meet this rule in our training samples.

The black smoke is usually located at the back of the smoky vehicle. Therefore, we focus the analysis on this region and call it the key region. More specifically, the key region from a detected vehicle object is determined by the following way. The height of the key region is adaptive and obtained by a linear fitting from a large number of labeled data to adapt to different distances between the vehicle and the camera. The horizontal width of the key region is related to the bounding box of the detected vehicle object, and it is set to the 0.8 times of the horizontal width of the bounding box, i.e., the horizontal width of the red box is 0.8 times of the horizontal width of the green box (as shown in Fig.2). This is an empirical value obtained through sufficient experiments. The horizontal coordinate of the bottom boundary of the key region is set to the horizontal coordinate of the bottom boundary of the bounding box of the detected vehicle object. The vertical coordinate of the center of the key region is set to the vertical coordinate of the center of the bounding box of the detected vehicle object. By this way, a vehicle object uniquely corresponds to a key region. Fig.2 is a sketch map used to understand the concept of the key region (marked by the red box).

Fig.3 shows three detected key regions in the real scene. We can see that, if the current vehicle is a smoky vehicle, the key region contains the black smoke most, and if the
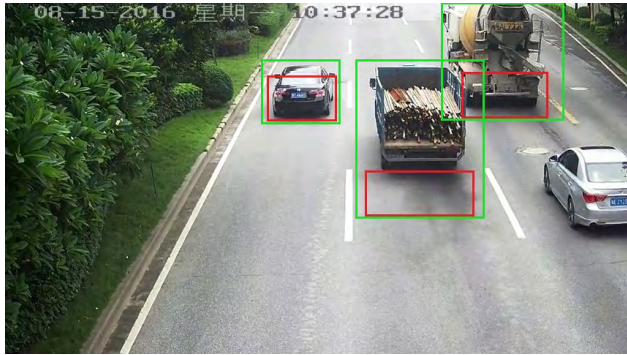
FIGURE 3. An original image from the surveillance video. The green box represents the bounding box of the moving object. The red box represents the positions of the key regions, including one smoky vehicle and two non-smoke vehicles.

current vehicle is a non-smoke vehicle, the key region contains the rear of the vehicle body most.

III. THE PROPOSED THREE GROUPS OF FEATURES

In this section, we will introduce three groups of features, including CM, MOH and RF-TOP based features. The color information CM features are used as a preliminary sieve to filter out the samples that are obviously non-smoke regions. The other two group of features are combined to one feature vector to obtain motion information and spatiotemporal information of the key region.

A. COLOR MOMENTS (CM)

To distinguish smoky vehicles and non-smoke vehicles, color information is the most easy to think of. Color Moment (CM) is a supportive measurement which can be used to differentiate images based on the color feature. It can be basically determined by calculating the mean, standard deviation and skewness.

For a key region image, we convert it to image P in the YUV color space. Because the color information is mainly distributed in the lower moments. The top three moments are used to characterize the color distribution,

$$\mu_i = \frac{1}{N} \sum_{j=1}^{N} p_{i,j}, \quad i = 1, 2, 3. \tag{2}$$

$$\sigma_i = \left(\frac{1}{N} \sum_{j=1}^{N} \left(p_{i,j} - \mu_i \right)^2 \right)^{1/2}, \quad i = 1, 2, 3. \tag{3}$$

$$s_i = \left(\frac{1}{N} \sum_{j=1}^{N} \left(p_{i,j} - \mu_i \right)^3 \right)^{1/3}, \quad i = 1, 2, 3. \tag{4}$$

where $p_{i,j}$ denotes the intensity value of the jth pixel with ith color channel component. N denotes the pixels number in image P. μ_i, σ_i and s_i denote the first, second and third color moments, respectively.

We connect the three moments with different color channels to form into one feature vector F_{CM},

$$F_{CM} = \{\mu_1, \mu_2, \mu_3, \sigma_1, \sigma_2, \sigma_2, s_1, s_2, s_3\} \tag{5}$$

The color information F_{CM} is trained by a simple Support Vector Machine (SVM) classifier and then used as a preliminary sieve to filter out the samples that are obviously non-smoke regions. In this way, we can reduce the time consumption of subsequent feature extraction to improve the algorithm speed.

B. MOTION ORIENTATION HISTOGRAM (MOH) FEATURES

For a smoky vehicle, the key regions in continuous frames characterize the diffusion process of the black smoke. For a non-smoke vehicle, the key regions in continuous frames characterize the process of the forward motion of the vehicle body. Based on the considerations, we improved the common MOH and take it as the second group features.

We first calculate the motion history image (MHI) using the following formula,

$$MHI_{x,y,t} = \begin{cases} \omega, & \text{if } D_{x,y,t} = 1 \\ \max\left\{0, MHI_{x,y,t-1} - 1\right\}, & \text{otherwise} \end{cases} \tag{6}$$

where $MHI_{x,y,t}$ denotes the intensity value of the motion history image at position (x, y) in tth frame. ω denotes the size of the time window, $D_{x,y,t} = 1$ denotes that the pixel at position (x, y) in tth frame is a moving object pixel.

And then we calculate the motion orientation of each point in MHI.

$$\theta_{x,y} = \arctan \frac{\mathrm{d}MHI_{x,y}/\mathrm{d}y}{\mathrm{d}MHI_{x,y}/\mathrm{d}x} \tag{7}$$

where $\theta_{x,y}$ denotes the motion orientation at position (x, y), $MHI_{x,y}$ denotes the intensity value of the motion history image at position (x, y).

We evenly quantize the motion orientation $0° \sim 180°$ to K bins, and then count the number that the motion orientation θ falling into each bin. Thus the motion orientation histogram (MOH) features are obtained.

$$MOH = \{n_1, n_2, \ldots, n_K\} \tag{8}$$

where $n_i (i = 1, 2, \ldots, K)$ denotes the number that falling into the ith bin. In this paper K is set to 9 and the bin step is $20°$.

However, the motion orientation may have small differences for different vehicles in the same road. In order to reduce intra-class distance, the MOH features should have the rotation invariance. Considering the characteristics of the smoky vehicle detection task, we propose the improved MOH features. We add the main orientation of the moving vehicle into the motion orientation θ to reduce noise and the intra-class distance. The main orientation can be given by,

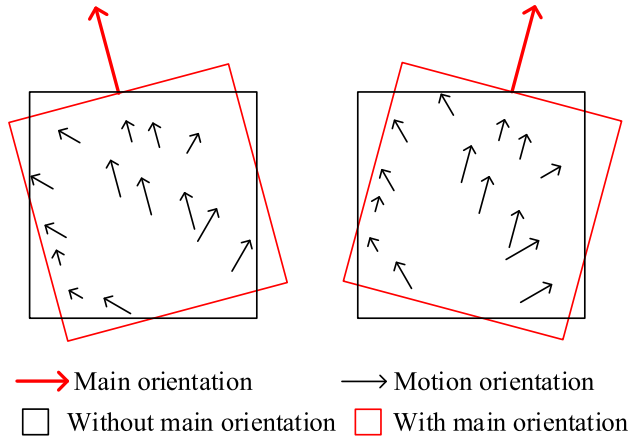$$\theta_{main}(t) = \arctan \frac{y_{center}(t) - y_{center}(t-1)}{x_{center}(t) - x_{center}(t-1)} \tag{9}$$

FIGURE 4. A sketch map to understand the difference to calculate the original MOH features and the improved MOH features.

FIGURE 5. A sketch map to understand the three orthogonal planes.

where $(x_{center}(t), y_{center}(t))$ and $(x_{center}(t - 1), y_{center}(t - 1))$ are the center coordinate of the bounding box of the detected moving object in the tth frame and $(t - 1)$th frame, respectively.

The improved MOH features, which denotes by F_{MOH}, can be given by,

$$F_{MOH} = \{n_p, n_{p+1}, \ldots, n_K, n_1, n_2, \ldots, n_{p-1}\} \quad (10)$$

$$p = \left\lceil \frac{\theta_{main}}{\theta_{bin}} \right\rceil \quad (11)$$

where θ_{bin} denotes the width of the bin.

Fig.4 shows the differences to calculate the original MOH features and the improved MOH features. Actually if we take the main motion orientation as the reference orientation, the two motion orientation images are the same. Otherwise, the two original motion orientation images are different. In a word, the improved MOH features have rotation invariance, and this characteristic is needed in smoky vehicle detection.

C. RANGE FILTERING ON THREE ORTHOGONAL PLANES (RF-TOP)

In this section, we will introduce the proposed RF-TOP based features, which used to characterize the key region at the back of the detected vehicle objects. Two strategies including histogram and projection are designed to extract discriminative dynamic features.

The Range Filtering (RF) [21] is a simple and efficient filtering operation. It can output an image where each output pixel contains the range value (maximum value - minimum value) of a small neighborhood NHOOD around the corresponding pixel in the original image. NHOOD is an odd multidimensional array fuelled with 0 and 1 where the nonzero elements specify the neighborhood for the range filtering operation. In range filtering, we also use the morphological dilation operation and erosion operation to determine the maximum and minimum values in the specified neighborhood.
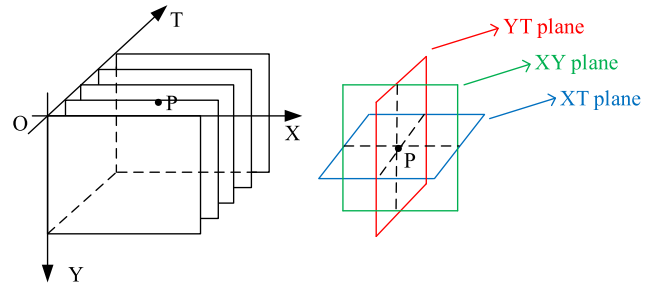
In the smoky vehicle detection task, we consider to extract features from the range filtering because of two factors. One is its high calculation efficiency. Another is that the smoke has smooth effects on the key region and makes the edge non-obvious, and the range filtering can obtain the edge information of the original image and also characterize the features of a local neighborhood. If the current vehicle is a smoky vehicle, the key region will have little edge information, and if the current vehicle is a non-smoke vehicle, the key region will have abundant edge information.

However, the original range filtering only consider the two-dimension (2D) image. To extend it to three dimension (3D) space and use the spatiotemporal information of the key region, we proposed the Range Filtering on Three Orthogonal Planes (RF-TOP), and two strategies including histogram and projection are designed to extract discriminative dynamic features.

For a key region, we collect the front N_{bef} frame and the back N_{aft} frame along the time axis in the same corresponding position to form a dynamic key images sequence. We set three coordinate axes (axis X, axis Y, and axis T) on this small video sequence of the key regions (as shown in Fig.5), and consider it as a stack of XY planes in axis T, a stack of YT planes in axis X, and a stack of XT planes in axis Y, respectively. The XT and YT planes can provide the information of space-time transitions.

For each pixel, we extract the three range values independently from three orthogonal planes. The image in XY plane shows the spatial features, the image in XT plane can give the visual impression of one row changing in time, and the image in YT plane can describe the motion of one column in temporal space. The range filtering code is extracted from the XY, XT and YT planes, which are denoted as XY−RF, XT−RF and Y T−RF. For all pixels, statistics of three different planes are obtained, and then concatenated to form one feature vector.

It is not reasonable obviously that we set the NHOOD in the time axis to be equal to the NHOOD in the space axis. Therefore, in the XT and YT planes, different NHOODs are assigned to sample neighboring points in space and time. With this approach the traditional square sampling is extended to rectangle sampling, as shown in Fig.6.

Let $X \times Y \times T$ denote the size of the key region sequences. Let (x_c, y_c, t_c) denote the coordinates of the center pixel
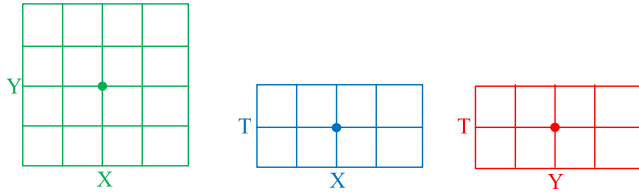
FIGURE 6. A sketch map of different NHOODs used in the XY, XT and YT planes.

$x_c \in \{0, 1, \ldots, X-1\}$, $y_c \in \{0, 1, \ldots, Y-1\}$, $t_c \in \{0, 1, \ldots, T-1\}$. Let $RF - TOP_{P_{XY},P_{XT},P_{YT}}$ denotes the RF distribution for this extracted 3D space.

Two strategies, including histogram and projection, are designed to extract discriminative dynamic features from $RF - TOP_{P_{XY},P_{XT},P_{YT}}$.

(1) Histogram

The histogram features can be defined as,

$$H_{i,j} = \sum_{x,y,t} c(x, y, t, i, j),$$
$$i = 0, 1, \ldots, n_j - 1; \ j = 0, 1, 2. \quad (12)$$

$$c(x, y, t, i, j) = \begin{cases} 1, & f_j(x, y, t) = i \\ 0, & \text{otherwise.} \end{cases} \quad (13)$$

where n_j denotes the number of different range values by the range filtering operator in the jth plane ($j = 0 : XY, j = 1 : XT$, and $j = 2 : YT$). $f_j(x, y, t)$ denotes the RF code of central pixel (x, y, t) in the jth plane. $H_{i,j}$ denotes the ith element of the histogram in the jth plane. $c(x, y, t, i, j)$ is a function related to parameters (x, y, t, i, j).

We normalized the above histograms to get the third group features $F_{RF-TOP-H}$,

$$F_{RF-TOP-H}^{i,j} = \frac{H_{i,j}}{\sum_{k=0}^{n_j-1} H_{k,j}} \quad (14)$$

where $F_{RF-TOP-H}^{i,j}$ denotes the ith element of the histograms features in the jth plane. It is easy to understand that the three histograms are concatenated to build a global description with the spatial and temporal features.

(2) Projection

The projection features can be defined as,

$$P_j = \sum_{k_j} f_j(x, y, t), \quad j = 0, 1, 2. \quad (15)$$

where P_j denotes the projection of the jth plane ($j = 0 : XY, j = 1 : XT$, and $j = 2 : YT$), $f_j(x, y, t)$ denotes the RF code of central pixel (x, y, t) in the jth plane, k_j denotes the jth coordinate axis ($k_0 : X$ axis, $k_1 : T$ axis, and $k_2 : Y$ axis).

We normalized the above projection features to get the third group features $F_{RF-TOP-P}$,

$$F_{RF-TOP-P}^{i,j} = \frac{P_j(i)}{\sum_k P_j(k)} \quad (16)$$

where $F_{RF-TOP-P}^{i,j}$ denotes the ith element of the projection features in the jth plane.

The idea of projection features are based on the reason that the smoke has a process from high concentration to low concentration in the direction from the vehicle exhaust hole to the road surface. To characterize the grey variation along this direction in the key region, the integral projection [22] is considered. It can describe the gray variation along a certain direction in the image. For non-smoke vehicles, the key region image sequences characterize the process that the vehicle disappears gradually. For smoky vehicles, the key region image sequences characterize the process that the smoke disappears gradually.

D. HOW TO USE THE THREE GROUPS OF FEATURES

In using the three groups of features, the color features F_{CM} are used as a preliminary sieve to filter out the samples that are obviously non-smoke regions. In the real surveillance videos, the number of non-smoke vehicles is much more than the smoky vehicles, and a preliminary filtering strategy is adopted to improve the algorithm speed.

The other two groups of features are combined to one feature vector to obtain motion information and spatiotemporal information of the key region. Two combination methods, including $(F_{MOH} + F_{RF-TOP-H})$ and $(F_{MOH} + F_{RF-TOP-P})$ are adopted and tested.

IV. PRUNING RADIAL BASIS FUNCTION NEURAL NETWORK (P-RBFNN) CLASSIFIER

In this section, we will introduce the training and classification of the P-RBFNN which used to classify smoky vehicles and no-smoke vehicles.

Radial basis function neural network (RBFNN) [23] is a commonly used three-layer feedforward networks including an input layer, a hidden radial basis layer and an output layer. Gaussian function is used as the transfer function in the hidden layer and a pure linear function is used as the activation function in the output layer. It can be used for function approximation and classification. RBFNN has physiological basis, more concise structure and faster learning speed.

The pruning method is to construct a large enough neural network first, and then get a simple neural network structure by deleting or merging some nodes or weights in training to improve generalization ability. We calculate the sensitivity (the contribution of the node or connection weight to the network error), and delete those nodes or weights with low values. The pruning algorithm can be divided into the following steps.

(a) Selected learning rate $\alpha_{learning}$, maximum iterations $k_{\max}$, continuous analysis number L, and threshold β_0

(b) Training the multilayer RBFNN shown in Fig.7(a) with standard training algorithm;

(c) Calculating sensitivity ρ_i of each node (hidden node or input node) according to formula (4),

$$\rho_i = E_{withoutUnit-i} - E_{withUnit-i} \quad (17)$$

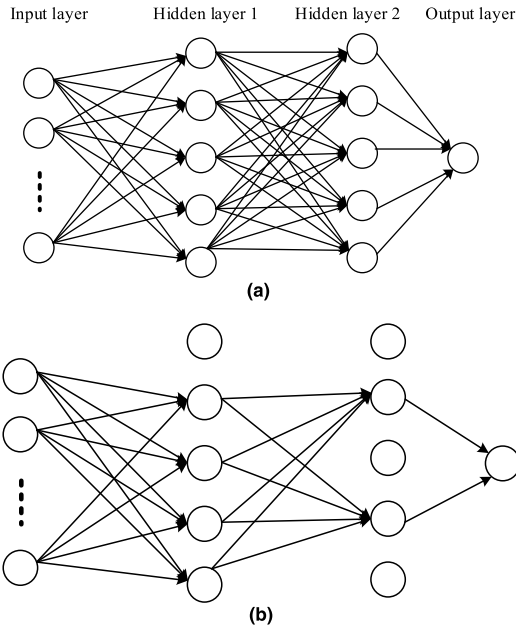where E_* is the training error of the neural network.

FIGURE 7. The pruning radial basis function neural network. (a) The original multilayer RBFNN structure. (b) The multilayer RBFNN structure after neural pruning.

(d) Calculating the mean $\bar{\rho}_i$ and standard deviations V_i of the normalized sensitivity $\hat{\rho}_i$ from continuous iterations L of each node (hidden node or input node). The calculation formulas are given by,

$$\hat{\rho}_i = \frac{\rho_i}{\sum_i |\rho_i|}. \tag{18}$$

$$\bar{\rho}_i = \frac{1}{L}\sum_{k=1}^{L}\hat{\rho}_i(t-k), \quad \bar{\rho}_i = \sqrt{\frac{1}{L}\sum_{k=1}^{L}\left(\hat{\rho}_i(t-k)-\bar{\rho}_i\right)^2} \tag{19}$$

(e) If the training error is less than the specified value, the value $|\bar{\rho}_i| + V_i$ of node i is minimal and $|\bar{\rho}_i| + V_i < \beta_0$, we should delete node i, otherwise turn (a);

(f) If the training exceeds the maximum number, it is over; otherwise, turn (b).

We use the features extracted from the training dataset to train the RBFNN. Fig.7(a) and Fig.7(b) show the original multilayer RBFNN structure and the pruning multilayer network structure. We can see that some nodes and connection weights are deleted. The advantage is to avoid overfitting. This design is based on the characteristics of the extracted feature vectors. In this way the multilayer pruning radial basis function neural network classifier (P-RBFNN) can be designed. We input the final feature extracted in Section III to the neural network shown in Fig.7(b), thus the input vector has the same number of the nodes of input layer, corresponding to one scalar output to make classifications.

V. EXPERIMENTS AND ANALYSIS

In this section, sufficient experiments will be made. The experiments are executed on the computer with Core(TM) 2 Duo2.40 GHz processor and VS2012 with OpenCV 2.4.9.

MATLAB R2015b is also used in the final part of classification.

A. DATASET

There are two datasets used in this paper, a testing dataset and a training dataset. Currently the testing vehicle database (SEU-SmokeVeh) contains 4 long videos and 98 short videos. Each long video has many no-smoke vehicles and $1 \sim 4$ smoky vehicles, and each short video has 1 smoky vehicle and $1 \sim 10$ non-smoke vehicles. These videos totally have 157550 frames, including 151613 non-smoke frames and 5937 smoky frames. These videos totally have 3521 vehicles, including 104 smoky vehicles and 3417 no-smoke vehicles. Most videos are with the resolution of 1920x1080 pixels, and in the testing they are all resized to 768x432 pixels using bilinear interpolation. This is a trade-off in speed and smoke resolution. The surveillance videos are all filmed in daytime with sunny weather. Currently the training dataset contains 1000 smoky frames from 43 smoky vehicles and 1000 non-smoke frames from 43 non-smoke vehicles. They are obtained with the same illumination conditions of the testing data and labeled by manual annotation. It should be noted that the training dataset and the testing data are not the same.

B. COMPARISONS OF DIFFERENT METHODS ON FRAME SEQUENCES

To verify the effectiveness and advantages of the proposed method, we first make comparisons with the smoky vehicle detection methods in [6] and [7]. In addition, some of the state-of-the-art smoke and fire detection methods [24]–[28], [30] are also selected to make comparisons. It should be noted that not all smoke or fire detection method can be directly transplanted into the smoky vehicle detection, since smoky vehicle detection is different with the common smoke and fire detection. To transplant the methods [24]–[29] into the smoky vehicle detection, some changes are needed. In our implementations of the block-based methods in [24]–[26], the block size is set to 24×24 pixels. If there is one or more blocks being detected as smoky blocks, the current frame will be classified as a smoky frame. It should be noted that the concept of the smoky frame is the frame with one or more smoky vehicles in current frame. In our implementations of the methods in [27]–[29], the part of the moving object detection all uniformly adopts the ViBe background subtraction algorithm used in this paper to facilitate comparisons.

The testing dataset SEU-SmokeVeh has 151613 non-smoke frame sequences and 5937 smoky frame sequences. Let γ_{smoke} and $\gamma_{non-smoke}$ denote the probability of correct classification (Pcc) of the smoky frames and the non-smoke frames, respectively. The evaluation criteria Pcc is defined as the rate between the number of the correct classification samples and the number of the total samples.

Table 1 shows the experimental results of different methods on frame sequences. The proposed method 1 and method 2

TABLE 1. Experiment results of different methods on frame sequences.

Different methods	γ_{smoke}	$\gamma_{non-smoke}$
Method in [24]	0.8215	0.8219
Method in [25]	0.8496	0.8434
Method in [26]	**0.8592**	**0.8593**
Method in [27]	0.8299	0.8388
Method in [28]	0.8300	0.8262
Method in [29]	**0.8600**	**0.8656**
Method in [6]	0.8503	0.8419
Method in [7]	0.8523	0.8529
Our method 1	**0.8757**	**0.8764**
Our method 2	**0.8609**	**0.8680**

TABLE 2. Experiment results of different methods on vehicles in surveillance videos.

Different methods	λ_{smoke}	$\lambda_{non-smoke}$
Method in [25]	0.8462	0.8443
Method in [26]	0.8558	0.8589
Method in [29]	**0.8654**	**0.8619**
Method in [6]	0.8462	0.8405
Method in [7]	0.8558	0.8531
Our method 1	**0.8750**	**0.8733**
Our method 2	**0.8654**	**0.8639**

use the features ($F_{MOH} + F_{RF-TOP-H}$) and features ($F_{MOH} + F_{RF-TOP-P}$), respectively. We can see that the proposed method 2 has a higher Pcc than the other methods. Methods [24]–[26] all used the local binary pattern (LBP) based texture features or its variants. However, the smoke has large changes in color and shape, and it is textureless (unlike rock, floor). In addition, methods [24], [26] do not use the dynamic features and this makes them easily with false alarms. Methods [27], [28] all used the dynamic features. However, in [27] identifying cone geometry feature is not applicable to smoky vehicle detection, and the used VO-GLCM (Variable Orientation Gray Level Co-occurrence Matrix) features is based on the fact that the variation of adjacent pixel color along smoke orientation is less than that of smoke verticality orientation. This fact is not obvious in the smoky vehicle detection. In [28], the histogram of oriented optical flow (HOOF) is extracted as a temporal feature based on the fact that the direction of smoke diffusion is upward owing to the thermal convection. However, this assumption makes it ineffective in smoky vehicle detection, since the smoke in our task does not go upward, and the HOOF features of the vehicle also will interfere with the features of the smoke. To our most surprise is that the deep-features-based method [29] is still not as good as our method. We collect and analyze the wrong classifications of method [29], and find that for the heavy-smoke images with abundant information of smoke boundary, the method [29] has a good performance. However, for the images with light smoke, it performs a little bad than our method. Method [6], [7] all did not use the dynamic features and this makes them easily with false alarms.

C. COMPARISONS OF DIFFERENT METHODS ON VIDEOS
The testing dataset SEU-SmokeVeh contains 3521 vehicles, including 104 smoky vehicles and 3417 non-smoke vehicles. In continuous k_1 frames, we assume k_2 frames is recognized

as smoky frame. If the following two rules are satisfied, the current frame sequences will be judged to have smoky vehicles,

$$\begin{cases} \text{Rule 1}: & k_2 > \xi_1 \\ \text{Rule 2}: & k_2/k_1 > \xi_2 \end{cases} \quad (20)$$

where ξ_1 and ξ_2 are two thresholds used to control detection results according to user's need.

Let λ_{smoke} and $\lambda_{non-smoke}$ denote the evaluation criteria Pcc of the smoky vehicles and the non-smoke vehicles, respectively. We only make comparisons with the top five methods. Table 2 shows the experimental results of different methods on vehicles in surveillance videos. We can see that the proposed method 1 also performs better than all the other methods.

Precision-Recall (PR) [30] curve has been widely used in automatic classification, information retrieval, recommender systems and social network analysis. In binary classification, it can characterize a better performance of automated systems when the classes are highly imbalanced, and the area under the precision-recall curve has been suggested as a performance measure. The testing dataset is imbalanced, and so we choose PR curves to characterize the algorithm performance.

The Precision and Recall are calculated by the following formulas,

$$\text{Precision} = \frac{TP}{TP + FP}, \quad \text{Recall} = \frac{TP}{TP + FN} \quad (21)$$

where TP is the number of smoky vehicles which been predicted as smoky vehicles, FN is the number of smoky vehicles which been predicted as no-smoke vehicles. FP is the number of no-smoke vehicles which been predicted as smoky vehicles.

Fig.8 shows the results of the PR curves of different methods by setting $\xi_1 = 50, 25, 15, 10, 8, 6, 4, 2; \xi_2 = 0.5$. The top three method [26, 29, 7] are used as baselines to make comparisons. We can see that the proposed method also performs better than the other three methods and has lower false alarm rates.

TABLE 3. Experiment results of different classifiers on frame images.

Different classifiers	γ_{smoke}	$\gamma_{non-smoke}$
BPNN	0.8637	0.8609
RBFNN	0.8650	0.8599
SVM-linear	0.8686	0.8698
SVM-rbf	**0.8725**	**0.8717**
P-RBFNN in method 1	**0.8757**	**0.8764**

TABLE 4. Effects on the algorithm performance of different moving object detection methods on frame sequences.

Different methods	λ_{smoke}	$\lambda_{non-smoke}$
AGMM in [31]	0.8738	0.8740
CodeBook in [32]	0.8730	0.8738
SOBS in [33]	0.8749	0.8748
SACON in [34]	0.8730	0.8729
PBAS in [35]	0.8751	0.8746
KDE in [36]	0.8728	0.8735
Vibe in [18] in method 1	0.8750	0.8739

FIGURE 8. PR curves of different methods.

FIGURE 9. Local screenshots of two correct detected smoky vehicles with poor vehicle detection. The green box represents the bounding box of the foreground object. The red box represents the key region at the back of the vehicle. (a) A correct detected smoky vehicle with serious poor vehicle detection. (b) A correct detected smoky vehicle with poor vehicle detection.

FIGURE 10. Some smoky vehicles captured from the surveillance videos. The green box represents the bounding box of the foreground object. The red box represents the key region at the back of the vehicle. (a) One smoky vehicle. (b) Local screenshots of 3 smoky vehicles.
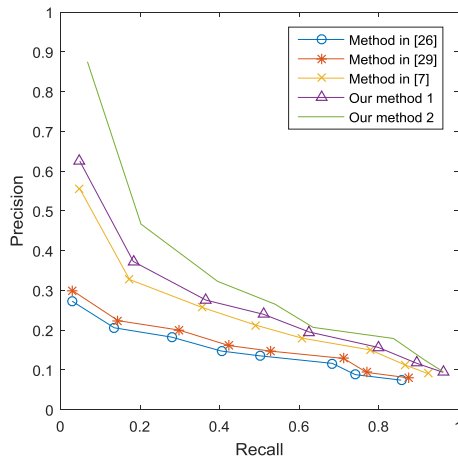
D. COMPARISONS OF DIFFERENT CLASSIFIERS

To verify the advantages of the P-RBFNN classifier used in this paper, we make comparisons with some widely-used classifiers, including back-propagation neural network (BPNN) classifier, radial basis function neural network (RBFNN) classifier, support vector machine with linear kernel function (SVM-linear) classifier, and support vector machine with radial basis function kernel function (SVM-rbf) classifier.

BPNN: The used BPNN has four layers. The nodes number of the input layer is set to the dimension of the feature vector. The hidden layer 1 and hidden layer 2 are all have 5 nodes.
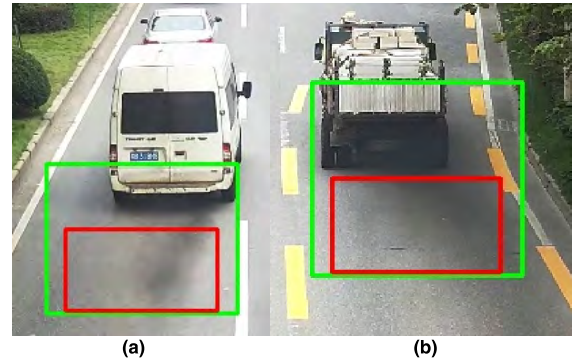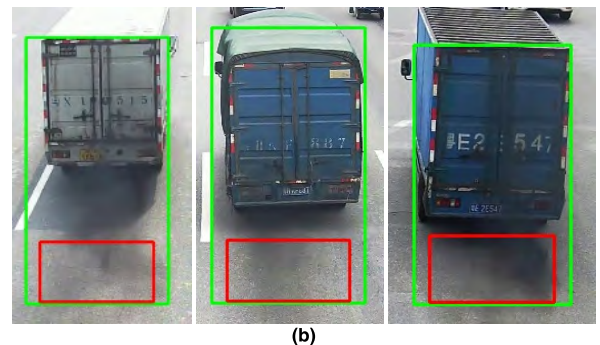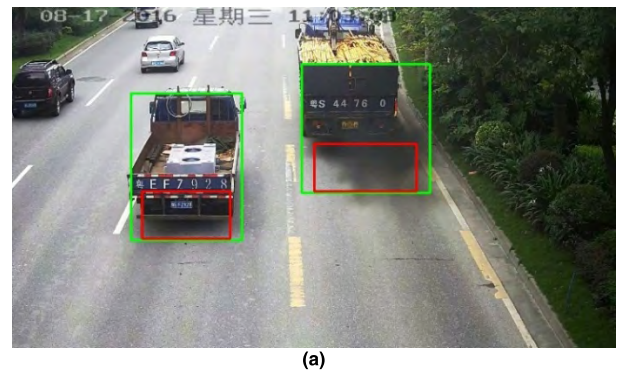
The output layer has one node. The activation function of the output layer adopts sigmoid function.

RBFNN: The RBFNN has four layers, and each layer has the same node number with the BPNN. The activation function of the hidden layers adopts Gaussian function.

SVM-linear: The linear function is used as kernel function (existing function *fitcsvm* in MATLAB R2015b).

SVM-rbf: The radial basis function is used as kernel function (existing function *fitcsvm* in MATLAB R2015b).

Table 3 shows the experimental results of different classifiers. We can see that the P-RBFNN classifier and the
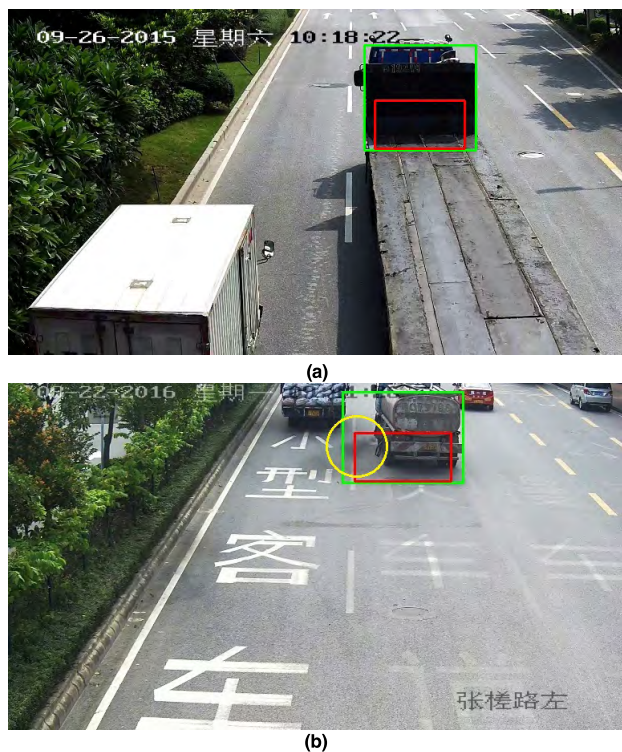
(a)

(b)

FIGURE 11. Two experimental results of false positives and missed detections. The green box represents bounding box of the vehicle object. The red box represents the key region. The yellow circle is the area with black smoke. (a) is a false positive. (b) is a missed detection.

SVM-rbf classifier achieve the higher Pcc than the other classifiers. Compared with the original RBFNN classifier, the Pcc has an important improvement after pruning.

E. COMPARISONS OF DIFFERENT MOVING OBJECT DETECTION METHODS

In this paper, we use the Vibe background subtraction algorithm to detect moving object. To verify the effects on the algorithm performance of different moving object detection methods, we choose the common methods, including AGMM [31], CodeBook [32], SOBS [33], SACON [34], PBAS [35], KDE [36],Vibe [18], and make comparisons to investigate the effects on the algorithm performance.

Table 4 shows the experimental results of different methods on frame sequences in surveillance videos. We can see that different moving object detection methods did not have obvious differences on the effects on the algorithm performance, and they all with the Pcc about 87.3-87.5%.

Fig.9 shows two examples of the correct recognized smoky vehicles but with poor moving object detection. We can see that, if it is analyzed from the perspective of moving object detection, the result in Fig.9 (a) is serious poor because of the interferences of the smoke, but the detected key region is just where the smoke in. Therefore, a poor moving object detection method will influence the moving object detection, but do not influence seriously on the smoky vehicle detection. From this we may be get the reasons of the results in Table 4 that different moving object detection methods did not have obvious differences on smoky vehicle detection.

Some experimental results of smoky vehicles captured from the surveillance videos are presented in Fig.10. From it we can see the effectiveness of our algorithm. The middle subimage in Fig. 10(b) shows a smoky vehicle with light smoke, and our method also correctly detect it.

A false positive and a missed detection are shown in Fig.11. They are all typical examples. In Fig.11(a), the head of this heavy truck is detected as a vehicle. It is a common problem of large objects detection that the moving object is incomplete. We can avoid this by heightening the position of the camera, but it is not good for license plate recognition (in this application we use the same camera to recognize license plates). Detecting errors does not directly result in recognition errors, but when the area is similar to black smoke, recognition errors will happen. In Fig.11(b), the vehicle belches black smoke from the left side of the vehicle. This situation is not many, but still exists, and this is also a deficiency of our algorithm. Our method can only deal with the vehicles that exhaust hole is in the vehicle rear.

VI. DISSCUSSION AND CONCLUSION

In this paper, we propose an automatic detection method of smoky vehicles in surveillance video based on RF-TOP and improved MOH to lower the false alarm rates. A new model called RF-TOP is proposed and used to characterize the key region at the back of the detected vehicle objects. Two strategies including histogram and projection are designed to extract discriminative dynamic features from RF-TOP. We also improve the original MOH features and propose the concept of main orientation to make the features have rotation invariance, which is needed in smoky vehicle detection. Three groups of features, including CM, improved MOH and RF-TOP based features are designed to obtain the color information, motion information and spatiotemporal information of the key region. For the traffic surveillance videos in the daylight with sunny weather, the proposed methods have better performances and work effectively with lower false alarm rates than existing smoky vehicle detection methods and related smoke detection methods, and the proposed method with histogram strategy achieves the best performance. It should be noted that the proposed works well for daylight and sunny weather, and the foggy weather may affect the algorithm performance.

Our method has the following advantages: remote monitoring, do not impede traffic, on duty all day long, can adapt to two lane, multi-lane and a variety of other road environment. With the further improvement of the proposed method in the future, it can be used to form an online monitoring network to detect high pollution smoky vehicles in cities.

Although we have done some successes in smoky vehicle detection, there are still many challenges. Such as the detection of the vehicle with exhaust pipe being underneath the vehicle and the case that the wind blows off the smoke immediately. All of above factors will reduce the accuracy of the smoky vehicle detection. Therefore, more works should be done in the future to improve the robustness.

REFERENCES

[1] S. Bujak-Pietrek, U. Mikolajczyk, I. Kaminska, M. Cieslak, and I. Szadkowska-Stanczyk, "Exposure to diesel exhaust fumes in the context of exposure to ultrafine particles," *Int. J. Occupational Med. Environ. Health*, vol. 29, no. 4, pp. 667–682, 2016.

[2] R. J. Laumbach and H. M. Kipen, "Acute effects of motor vehicle traffic-related air pollution exposures on measures of oxidative stress in human airways," *Ann. New York Acad. Sci.*, vol. 1203, pp. 107–112, Aug. 2010. [Online]. Available: http://europepmc.org/backend/ptpmcrender.fcgi?accid=PMC4043285&blobtype=pdf, doi: 10.1111/j.1749-6632.2010.05604.x.

[3] H. Liu, S. Chen, and N. Kubota, "Intelligent video systems and analytics: A survey," *IEEE Trans. Ind. Informat.*, vol. 9, no. 3, pp. 1222–1233, Aug. 2013.

[4] H. Liu, S. Y. Chen, and N. Kubota, "Guest editorial special section on intelligent video systems and analytics," *IEEE Trans. Ind. Informat.*, vol. 8, no. 1, p. 90, Feb. 2012.

[5] P. Pyykőnen, P. Peussa, M. Kutila, and K. Fong, "Multi-camera-based smoke detection and traffic pollution analysis system," in *Proc. IEEE 12th Int. Conf. Intell. Comput. Commun. Process. (ICCP)*, Cluj-Napoca, Romania, Sep. 2016, pp. 233–238.

[6] H. Tao and X. Lu, "Smoky vehicle detection based on multi-scale block Tamura features," *Signal, Image Video Process.*, vol. 12, no. 6, pp. 1061–1068, Sep. 2018.

[7] H. Tao and X. Lu, "Smoky vehicle detection based on multi-feature fusion and ensemble neural networks," *Multimedia Tools Appl.*, pp. 1–25, Jun. 2018, doi: 10.1007/s11042-018-6248-2.

[8] F. Yuan, "A fast accumulative motion orientation model based on integral image for video smoke detection," *Pattern Recognit. Lett.*, vol. 29, no. 7, pp. 925–932, 2008.

[9] O. Gunay, B. U. Toreyin, K. Kose, and A. E. Çetin, "Entropy-functional-based online adaptive decision fusion framework with application to wildfire detection in video," *IEEE Trans. Image Process.*, vol. 21, no. 5, pp. 2853–2865, May 2012.

[10] T.-H. Chen, P.-H. Wu, and Y.-C. Chiou, "An early fire-detection method based on image processing," in *Proc. Int. Conf. Image Process.*, 2004, pp. 1707–1710.

[11] B. U. Töreyin, Y. Dedeoğlu, and A. E. Çetin, "Wavelet based real-time smoke detection in video," in *Proc. 13th Eur. Signal Process. Conf.*, Sep. 2005, pp. 293–296.

[12] H. Tian, W. Li, P. O. Ogunbona, and L. Wang, "Detection and separation of smoke from single image frames," *IEEE Trans. Image Process.*, vol. 27, no. 3, pp. 1164–1177, Mar. 2018.

[13] H. Tian, W. Li, L. Wang, and P. O. Ogunbona, "A novel video-based smoke detection method using image separation," in *Proc. IEEE Int. Conf. Multimedia Expo*, Jul. 2012, pp. 532–537.

[14] H. Tian, W. Li, L. Wang, and P. Ogunbona, "Smoke detection in video: An image separation approach," *Int. J. Comput. Vis.*, vol. 106, no. 2, pp. 192–209, 2014.

[15] S. R. E. Datondji, Y. Dupuis, P. Subirats, and P. Vasseur, "A survey of vision-based traffic monitoring of road intersections," *IEEE Trans. Intell. Transp. Syst.*, vol. 17, no. 10, pp. 2681–2698, Oct. 2016.

[16] R. A. Hadi, G. Sulong, and L. E. George, "Vehicle detection and tracking techniques: A concise review," *Signal Image Process.*, vol. 5, no. 1, pp. 1–12, 2014.

[17] N. C. Mithun, T. Howlader, and S. M. M. Rahman, "Video-based tracking of vehicles using multiple time-spatial images," *Expert Syst. Appl.*, vol. 62, pp. 17–31, Nov. 2016.

[18] O. Barnich and M. Van Droogenbroeck, "ViBe: A universal background subtraction algorithm for video sequences," *IEEE Trans. Image Process.*, vol. 20, no. 6, pp. 1709–1724, Jun. 2011.

[19] T. Chen and S. Lu, "Robust vehicle detection and viewpoint estimation with soft discriminative mixture model," *IEEE Trans. Circuits Syst. Video Technol.*, vol. 27, no. 2, pp. 394–403, Feb. 2015.

[20] V. D. Nguyen, H. Van Nguyen, D. T. Tran, S. J. Lee, and J. W. Jeon, "Learning framework for robust obstacle detection, recognition, and tracking," *IEEE Trans. Intell. Transp. Syst.*, vol. 18, no. 6, pp. 1633–1646, Jun. 2016.

[21] R. C. Gonzalez, R. E. Woods, and S. L. Eddins, *Digital Image Processing Using MATLAB*. Upper Saddle River, NJ, USA: Prentice-Hall, 2003, ch. 11.

[22] R. N. Bracewell, *Two Dimensional Imaging*. Englewood Cliffs, NJ, USA: Prentice Hall, 1995, pp. 505–537.

[23] T. Zheng and C. Wang, "Relationship between persistent excitation levels and RBF network structures, with application to performance analysis of deterministic learning," *IEEE Trans. Cybern.*, vol. 47, no. 10, pp. 3380–3392, Oct. 2017.

[24] F. Yuan, "Video-based smoke detection with histogram sequence of LBP and LBPV pyramids," *Fire Safety J.*, vol. 46, no. 3, pp. 132–139, Apr. 2011.

[25] G. Lin, Y. Zhang, Q. Zhang, Y. Jia, G. Xu, and J. Wang, "Smoke detection in video sequences based on dynamic texture using volume local binary patterns," *KSII Trans. Internet Inf. Syst.*, vol. 11, no. 11, pp. 5522–5536, 2017.

[26] F. Yuan, "A double mapping framework for extraction of shape-invariant features based on multi-scale partitions with AdaBoost for video smoke detection," *Pattern Recognit.*, vol. 45, no. 12, pp. 4326–4336, 2012.

[27] S. Wang, Y. He, H. Yang, K. Wang, and J. Wang, "Video smoke detection using shape, color and dynamic features," *J. Intell. Fuzzy Syst.*, vol. 33, no. 1, pp. 305–313, 2017.

[28] B. Ko, J. Park, and J.-Y. Nam, "Spatiotemporal bag-of-features for early wildfire smoke detection," *Image Vis. Comput.*, vol. 31, no. 10, pp. 786–795, Oct. 2013.

[29] Y. Luo, L. Zhao, P. Liu, and D. Huang, "Fire smoke detection algorithm based on motion characteristic and convolutional neural networks," *Multimedia Tools Appl.*, vol. 77, no. 12, pp. 15075–15092, 2018.

[30] P. A. Flach and M. Kull, "Precision-recall-gain curves: PR analysis done right," in *Proc. Int. Conf. Neural Inf. Process. Syst.* Cambridge, MA, USA: MIT Press, 2015, pp. 838–846.

[31] Z. Zivkovic, "Improved adaptive Gaussian mixture model for background subtraction," in *Proc. 17th Int. Conf. Pattern Recognit. (ICPR)*, vol. 2, Aug. 2004, pp. 28–31.

[32] K. Kim, T. H. Chalidabhongse, D. Harwood, and L. Davis, "Real-time foreground-background segmentation using codebook model," *Real-Time Imag.*, vol. 11, no. 3, pp. 172–185, Jun. 2005.

[33] L. Maddalena and A. Petrosino, "A self-organizing approach to background subtraction for visual surveillance applications," *IEEE Trans. Image Process.*, vol. 17, no. 7, pp. 1168–1177, Jul. 2008.

[34] H. Wang and D. Suter, "SACON: A consensus based model for background subtraction," Dept. Elect. Comput. Syst. Eng., Monash Univ., Clayton, VIC, Australia, Tech. Rep. MECSE-15-2005, 2005.

[35] M. Hofmann, P. Tiefenbacher, and G. Rigoll, "Background segmentation with feedback: The pixel-based adaptive segmenter," in *Proc. IEEE Comput. Soc. Conf. Comput. Vis. Pattern Recognit. Workshops*, Jun. 2012, pp. 38–43.

[36] A. Elgammal, D. Harwood, and L. Davis, "Non-parametric model for background subtraction," in *Proc. 6th Eur. Conf. Comput. Vis. (ECCV)*, Dublin, Ireland. New York, NY, USA: Springer-Verlag, Jun./Jul. 2000, pp. 751–767.

HUANJIE TAO received the B.S. degree in mathematics and applied mathematics from Xinxiang University, Xinxiang, China, in 2013, and the M.S. degree in mathematics and information science from Capital Normal University, Beijing, China, in 2016. He is currently pursuing the Ph.D. degree in pattern recognition and intelligent system with Southeast University, Nanjing, China. His current research interests include image processing, computer vision, feature extraction, deep learning, and pattern recognition.
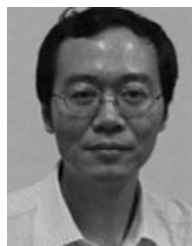
XIAOBO LU received the B.S. degree from Shanghai Jiao Tong University, Shanghai, China, the M.S. degree from Southeast University, Nanjing, China, and the Ph.D. degree from Nanjing University of Aeronautics and Astronautics. He did his postdoctoral research with Chien-Shiung Wu Laboratory, Southeast University, from 1998 to 2000. He is currently a Professor with the School of Automation and the Deputy Director of the Detection Technology and Automation Research Institute, Southeast University. He has co-authored the book *An Introduction to the Intelligent Transportation Systems* (Beijing: China Communications, 2008). His research interests include image processing, signal processing, pattern recognition, and computer vision. He received many research awards, such as the First Prize in the Natural Science Award from the Ministry of Education of China and the prize in the Science and Technology Award of Jiangsu province.

● ● ●